physics

MDPI

*Article*

# Influence of Three-Body Recombination on Formation of Dark Atoms

**Dmitry Kalashnikov * and Konstantin Belotsky**

Department of Elementary Particle Physicsand, National Research Nuclear University MEPhI (Moscow Engineering Physics Institute), Kashirskoe Shosse 31, Moscow 115409, Russia; k-belotsky@yandex.ru
* Correspondence: dskalashnikov@mephi.ru

**Abstract**

As is known, the standard cosmological model (ΛCDM) demonstrates reasonable agreement with observations of the large-scale structure of the Universe. However, the model shows significant differences between observations of individual galaxies and numerical simulations. To address these discrepancies, various extensions of ΛCDM are being explored, one of which is self-interacting dark matter (SIDM). We employ a SIDM model characterized by a dark Coulomb-like interaction between dark electrons and dark protons and mediated by a dark photon. An essential feature of such models is recombination—the formation of 'dark atoms', which can be part of dark matter (DM). The spatial distributions of two-component DM that may explain the positron anomaly have been studied in earlier studies. Our contribution is to calculate three-body recombination rates and the resulting neutral fraction of 'dark atoms', as well as to show that the recombination process provides a natural mechanism for generating such two-component DM during the evolution of the Universe.

**Keywords:** dark matter; SIDM; positron anomaly; three-body recombination

## 1. Introduction

In the modern standard cosmological model (ΛCDM), the Universe is filled with baryonic matter, dark energy, and cold non-interacting dark matter (CDM). The ΛCDM framework has successfully explained many large-scale structures and phenomena in the Universe, such as the cosmic microwave background radiation and the distribution of galaxies. However, it faces small-scale issues, notably the core–cusp problem [1] and the missing-satellites problem [2].

To resolve these issues, extensions to the ΛCDM have been proposed, including self-interacting dark matter (SIDM) models [3]. SIDM models suggest that interactions between dark matter (DM) particles lead to energy and momentum exchange, potentially explaining observed discrepancies in dark matter density profiles and galaxy formation [4–8].

Recent studies indicate that SIDM can also resolve the final parsec problem in supermassive black hole (SMBH) mergers, where conventional mechanisms fail to efficiently bring SMBH binaries close enough to merge through gravitational wave emission alone. The dynamical friction induced by SIDM around SMBHs reduces the inspiral timescale by allowing the dark matter spikes to act as reservoirs for the energy released from SMBH orbits, solving the final parsec problem as a result [9]. This effect is particularly significant when the ratio of the self-interaction cross-section to the mass of the DM particle, $\sigma/m$,



Received: 13 October 2025
Revised: 23 November 2025
Accepted: 25 November 2025
Published: 2 March 2026

is of the order of about 1 $cm^2/g$, which is comparable with that which needs to resolve small-scale structure issues [7] in CDM scenarios.

The positron anomaly, characterized by an excess of high-energy positrons in cosmic ray spectra, still remains an unsolved astrophysical puzzle. The positron excess was first observed by PAMELA [10] and confirmed by AMS [11] experiments. There have been attempts to solve it with the help of pulsars [12,13], as well as with scenarios with decaying or annihilating DM [14–20]. Both pulsar and DM explanations have their model difficulties. In the case of DM models, it is the overproduction of gamma radiation. This motivates the development of corresponding models, which we carried out with respect to the DM model.

Our DM model [18,19,21] involves a two-component DM scenario. The first component is supposed to be stable, non-interacting, and forms the dark matter halo that determines large-scale gravitational dynamics. The second component, in contrast, is self-interacting and includes decay (or annihilation) channels into Standard Model (SM) particles, such as positrons. Unlike the halo-forming component, the decaying component is characterized by a specific spatial distribution. This allows it serving a localized source of the observed positron excess while avoiding a contribution to the gamma-ray background (IGRB). This component is only a minor part of dark matter, concentrating in the Galaxy disk to avoid contradiction. In this paper, we demonstrate how two-component DM can naturally arise within SIDM models, without focusing on structure formation itself.

We consider a dark-sector U(1) model with a 'dark electron' of mass $m_a$ and heavier 'dark proton' of mass $m_b$, interacting with a dark photon mediator. This simplified model can lead to a two-component DM mixture through the recombination process. Recombination or annihilation of DM particles in cosmology is an essential process that influences the dynamic properties and thermodynamic evolution of the Universe [22–26]. Understanding this process is crucial because recombined particles are expected to form quite small dark atoms; these become collisionless and therefore behave like the first component. This is not the case for the DM particles that fail to recombine, which constitute the second, 'interacting' component.

In this study, we do not specify how the sector of DM particles is connected to the SM particles. For the purposes of our study here, it is sufficient to assume that the self-interacting component is weakly coupled to the SM through some interaction, for example, kinetic mixing between the dark and ordinary photons, a 'Higgs-portal' coupling, or others. Various realizations of such possibilities, together with their respective advantages and phenomenological constraints, have been extensively discussed in the literature [20,27–30]. This does not affect the recombination dynamics considered here and is therefore left outside the scope of the present study.

Since the dark U(1) gauge boson is massless, the associated $y$-radiation contributes to the effective number of relativistic species $N_{\rm eff}$, which is defined by epoch of Big Bang nucleosynthesis (BBN) (hereafter, symbol $y$ is attributed to dark U(1)-interaction and all interactions corresponding to it). However, the dark sector is supposed to decouple from the SM bath at decouple temperatures $T_{\rm dec} \gg T_{\rm BBN} \sim 1$ MeV, which leads to the contribution to total matter density, taking into account the entropy factor, at BBN, much less than 1, satisfying the current constraints. Estimation of a long-range $y$-interaction and its impact on $N_{\rm eff}$ can be found, for example, in Ref. [31].

Despite recent progress, current models still have issues in understanding the recombination processes involving SIDM. The main gap lies in the precise mechanisms through which SIDM recombines. Previous studies have employed Kramers recombination [23,26] and classical methods [32,33] to analyze these processes. Studies using Kramers' method have shown that the number of recombining particles remains low throughout the lifetime of the Universe in reasonable model parameters, indicating that less than 10% of DM particles form bound states under the model parameters described. This low recombination rate

leaves a relatively large fraction of DM charged, which significantly influences its dynamic properties. As a result, this imposes stronger constraints on the interaction cross-section of such particles [20]. The classical approach to recombination description requires an applicability check under cosmological conditions [33]. Our analysis, in contrast, uses the three-body recombination mechanism described by Lev Pitaevskii [34], which shows higher recombination rates under appropriate conditions.

In this paper, we examine the three-body DM recombination channel. We consider identifying differences with the aforementioned Kramers case regarding the rate and final composition of DM (fractions of DM atoms and free particles). This difference turns out to be significant, opening up new possibilities for understanding the behavior of DM and the evolution of large-scale structures.

## 2. Model and Definitions

### *2.1. Three-Body Recombination Mechanism*

Three-body recombination is a process where an electron, before forming a bound state with a proton, interacts with another particle—typically a neutral atom, ion, or electron. The interaction allows the electron to lose energy and form a bound state with the ion. This mechanism is extensively in plasma physics [35]. Since a complete theory of three-body processes is not available, practical calculations are based on approximations. Following Pitaevskii [34], we compute the electron–ion recombination rate $\beta = \langle \sigma v \rangle$ (with $v$ the relative velocity and the angular brackets denoting the thermal average over the velocity distribution) using a diffusion approximation:

$$\beta = \frac{32\sqrt{2\pi}}{3} \frac{m_a^{1/2} e^6 \sigma_t}{T_a^{5/2} m_b} n, \tag{1}$$

where $e$ is the dark-sector charge (with $4\pi\alpha_y = e_y^2$, where $\alpha_y$ is the interaction constant, and $e = e_y$ used below for consistency), $T_a$ is the electron temperature, $\sigma_t$ is the total electron elastic scattering cross-section on an atom, and $n$ is the atom number density. The following restriction on the limits of applicability of the formula was obtained:

$$T_e \ll e^2 n \sigma \sqrt{\frac{m_a}{m_b}}, \quad T_e \gg e^2 \sqrt{\frac{m_a}{m_b}} \Big/ R_a, \tag{2}$$

where $R_a$ is the length of scattering. The condition (2) identifies temperatures where three-body capture is effective and two-body processes do not dominate, and it requires a sufficiently high neutral density, for example, in the early Universe or in overdense regions.

### *2.2. Estimate of Number Density of Recombined Particles*

Here, we follow the calculation method [31] developed for U(1)-interacting dark matter in the form of hypothetical heavy neutrinos.

In the early Universe, when temperatures exceeded $m_a$, the processes of ionization and recombination are considered to be in chemical equilibrium. As the Universe expanded, $y$-electrons and $y$-protons cooled and formed bound states, and the gas became transparent to $y$-radiation as the freeze-out of $y$-photons occurred. It is assumed that decoupling took place at a recombination temperature $T_{\rm rec} \sim m_a/10$.

This assumption is based on a common estimate used for particles that behave similarly to neutral atoms. In such cases, the decoupling temperature is typically around 0.1 of the particle's mass, reflecting the point at which the thermal energy is no longer sufficient to keep the particles ionized. This estimation is consistent with similar processes observed in cosmology, such as the recombination of hydrogen.

After recombination, the $y$-photon background decouples from particles $a$ and $b$, as well as from ordinary matter. The temperature of the $y$-background ($T_y$) scales as $1/a(t)$, where $a(t)$is the cosmic scale factor. Due to minimal interaction, the influence of ordinary matter on the $y$-plasma is negligible.

Consequently, after decoupling from the $y$-background, the temperature of the $y$-particle gas evolves with the background temperature $T$ (and cosmic time $t$) as described by [23]

$$T_a \approx \frac{T^2}{T_{ay}}, \quad T_{ay} = 0.2 \text{ MeV} \left(\frac{m_a}{100 \text{ GeV}}\right)^{3/2} \frac{0.01}{\alpha_y}. \tag{3}$$

We assume kinetic equilibration between the light and heavy dark species after $y$-decoupling, $T_b \simeq T_a$. To calculate the change in the concentration of $y$-particles, we use the kinetic equation in an expanding Universe:

$$-\frac{\mathrm{d}n_a}{\mathrm{d}t} = \beta n_a n_b + 3Hn_a, \tag{4}$$

where $n_a$ and $n_b$ are, respectively, the concentrations of particles $a$ and $b$, $\beta$ denotes the recombination rate, and $H$ is the Hubble parameter. To achieve an electroneutral plasma, we assume that the number of particles $a$ and $b$ are the same: $n_a = n_b = n$. We get the equation

$$-\frac{\mathrm{d}n}{\mathrm{d}t} = \beta n^2 + 3Hn. \tag{5}$$

As the Universe expands, the concentration per unit volume continually drops. Furthermore, cosmic time ($t$) is an inconvenient variable for parameterizing the expansion scale in cosmology. Instead, it is far more convenient to use the scale factor ($a(t)$) or the ordinary photon cosmic microwave background (CMB) temperature ($T$). To simplify the subsequent analysis, we therefore adopt these alternative variables [36]:

$$r = n/s, \quad s \approx \frac{2\pi^2 g_s}{45} T^3, \quad -\mathrm{d}t = \frac{1}{HT}\,\mathrm{d}T, \tag{6}$$

where $s$ is the entropy density, $g_s$ is the number of degrees of freedom (standard formula depending on temperature with application of smoothing of transitions between different degree numbers). For three-body recombination, we have again Equation (1) for recombination rate $\beta$. Equation (5) can then be rewritten as

$$\frac{\mathrm{d}r}{\mathrm{d}T} = \frac{r^2 s}{HT}\beta(T_a) = \frac{32\sqrt{2\pi}}{3}\frac{r^3 s^2}{HT}\frac{m_a^{1/2} e_y^6 \sigma_T}{T_a^{5/2} m_b}. \tag{7}$$

For consistency with the three-body channel considered, we take the interaction to be electron–ion and use the transport cross-section $\sigma \equiv \sigma_T$ as Coulomb scattering $\sigma \sim e_y^4/T_a^2$. This choice of cross-section reflects the dominance of low-energy collisions in the early Universe, where the temperature is much lower than the binding energy of the particles, thus making this a suitable approximation for the processes under consideration.

Let us consider the relationship between the temperature of $y$-particles and CMB photons (3):

$$\frac{\mathrm{d}r}{\mathrm{d}T} = \frac{32\sqrt{2\pi}}{3} \cdot \frac{s^2 m_a^{1/2} e_y^{10} T_{ay}^{9/2}}{H m_b} \cdot \frac{r^3}{T^{10}}. \tag{8}$$

The Hubble parameter during radiation (RD) and matter domination (MD) is [31]

$$H(T) = \begin{cases} h_{\mathrm{RD}}\, T^2, & h_{\mathrm{RD}} = 5.5\sqrt{g_\epsilon/11}/M_{\mathrm{Pl}}, \\ h_{\mathrm{MD}}\, T^{3/2}, & h_{\mathrm{MD}} = 10^{-14}/M_{\mathrm{Pl}}^{1/2}, \end{cases} \tag{9}$$

where $h_{\mathrm{RD}}$ and $h_{\mathrm{MD}}$ are constants setting the Hubble rate during the RD and MD epochs, $g_\epsilon$ is the effective number of relativistic degrees of freedom for energy density and $M_{\mathrm{Pl}}$ is the Planck mass.

Substituting $s(T)$ and $H(T)$ into Equation (8), for the RD stage, we find

$$\frac{\mathrm{d}r}{\mathrm{d}T} = \frac{32\sqrt{2\pi}}{3} \cdot \frac{(2\pi^2 g_s/45)^2 m_a^{1/2} e_y^{10} T_{ay}^{9/2}}{h_{\mathrm{RD}} m_b} \cdot \frac{r^3}{T^6}. \tag{10}$$

By separating the variables and integrating with the initial conditions $r(T_{\mathrm{rec}}) = r_0$, one gets an expression for the relative density in the RD stage:

$$\frac{r_{\mathrm{RD}}(T)}{r_0} = \left[1 + \frac{2}{5} D_{\mathrm{RD}} r_0^2 \left(\frac{1}{T^5} - \frac{1}{T_{\mathrm{rec}}^5}\right)\right]^{-1/2}, \tag{11}$$

$$\text{with} \quad D_{\mathrm{RD}} = \frac{32\sqrt{2\pi}}{3} \frac{(2\pi^2 g_s/45)^2 m_a^{1/2} e_y^{10} T_{ay}^{9/2}}{h_{\mathrm{RD}} m_b}.$$

The transition from the RD stage to the MD stage occurred at radiation-to-matter (RM) $T_{\mathrm{RM}} \approx 1.2\,\mathrm{eV}$ and $r_{\mathrm{RM}} = r_{\mathrm{RD}}(T_{\mathrm{RM}})$. Then, having made similar calculations in the MD stage, one gets

$$r_{\mathrm{MD}}(T) = r_{\mathrm{RM}} \cdot \left[1 + \frac{4}{9} D_{\mathrm{MD}} r_{\mathrm{RM}}^2 \left(\frac{1}{T^{9/2}} - \frac{1}{T_{\mathrm{RM}}^{9/2}}\right)\right]^{-1/2}, \tag{12}$$

$$\text{with} \quad D_{\mathrm{MD}} = \frac{32\sqrt{2\pi}}{3} \frac{(2\pi^2 g_s/45)^2 m_a^{1/2} e_y^{10} T_{ay}^{9/2}}{h_{\mathrm{MD}} m_b}.$$

Equations (11) and (12) describe the evolution of the charged fraction as a function of the photon temperature across radiation- and matter-dominated epochs. In these variables, the applicability criterion for the three-body formula then reads

$$\frac{r}{r_0} \gg \frac{T_{ay}^2}{T^4} \left((4\pi\alpha_y)^3 r_0 \sqrt{\frac{m_a}{m_b}} (2\pi^2 g_s/45)\right)^{-1}. \tag{13}$$

## 3. Results

### *3.1. Numerical Analysis of Solution*

Here, we focus on a numerical analysis of solutions (11) and (12) to evaluate the impact of three-body recombination on the concentration of $y$-particles. We use the SIDM model discussed in Ref. [23] to compare the contribution from three-body recombination to the concentration of $y$-particles. Table 1 shows the parameters of the model we are considering (a closely related scenario with a massless dark photon and the same U(1) charge structure has recently been considered in Ref. [37]). In Ref. [23], the best-fit region corresponds to GeV-scale dark proton and MeV-scale dark electron masses with a larger dark coupling, based on different cosmological studies. In contrast, we study TeV-scale masses and the three-body recombination in a two-component dark sector, so the benchmark regions are essentially non-overlapping. A dedicated global fit is required for a quantitative comparison.

**Table 1.** Model parameters used in this study to analyze the number of recombined particles. See text for details.

| Parameter | Value |
|---|---|
| $m_a$ | 100 GeV |
| $m_b$ | 1 TeV |
| $\alpha_y = e_y^2/4\pi$ | 0.01 |
| $r_0 = \dfrac{\rho_{\mathrm{CMB}}}{s m_b}$ | $4.6 \cdot 10^{-13}$ |

Figures 1 and 2 show the results obtained for the relative density of charged $y$-particles as a function of the temperature of CMB photons (dependence on time or red shift can be straightforwardly obtained from the CMB temperature).

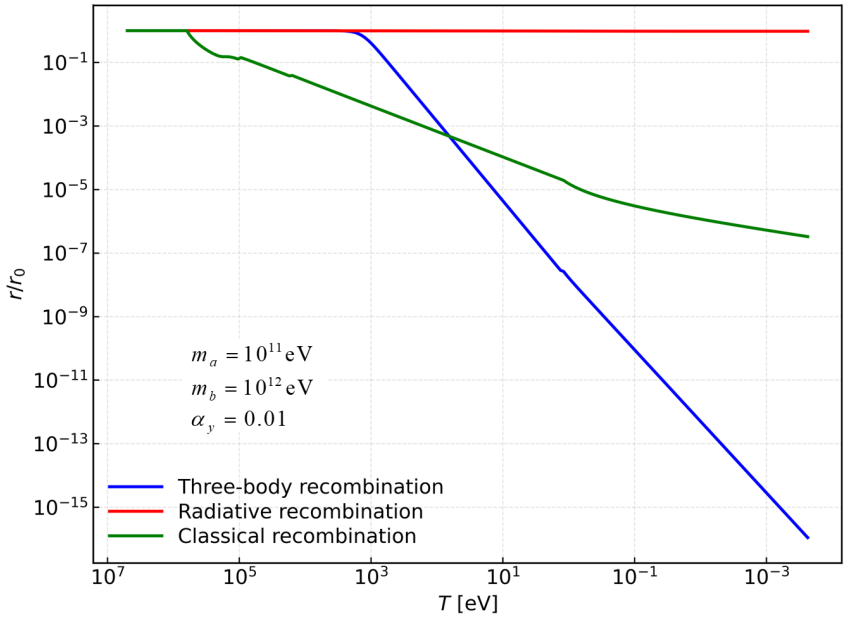


**Figure 1.** Relative density ($r/r_0$) of $y$-charged particles versus the CMB temperature $T$ (see Equation (11) and Table 1). Three different recombination mechanisms are compared: three-body recombination, radiative recombination, and classical recombination, as indicated. The results demonstrate that three-body recombination leads to a rapid decrease in the relative density of $y$-charged particles, with nearly all particles forming bound states by the present epoch ($T \approx 10^{-}3$ eV).

For the Kramers recombination formula (Figure 2), only a relatively small fraction of charged particles is expected to recombine by the present time ($T \approx 10^{-3}$ eV). This signifies that most of the plasma stays charged: it maintains the interaction between the particles.

Initial analysis suggests that the majority of plasma particles may recombine via the three-body recombination process. This mechanism has the potential to significantly increase the relative number of recombined particles, reaching up to $r/r_0 \sim 10^{-16}$, which implies that nearly all the particles form bound states. If the efficiency of this process agrees with these initial estimates, the process then leads to a rapid conversion of SIDM particles into states that mimic non-interacting CDM. However, to confirm the validity of these conclusions, it is essential to examine the applicability of the formulas used within the parameter space relevant to the physical conditions of interest.

Figure 3 illustrates the applicability constraint for the three-body recombination expression (11). The formula (11) is valid only when the relative density lies above the green line; the shaded region marks this domain. For the parameter set in Table 1, the charged fraction remains below the threshold (13) over the relevant temperature range. Under these

conditions, the three-body channel does not contribute significantly to the evolution of the charged density. The result may differ for alternative parameters of the model where three-body recombination can be applied.

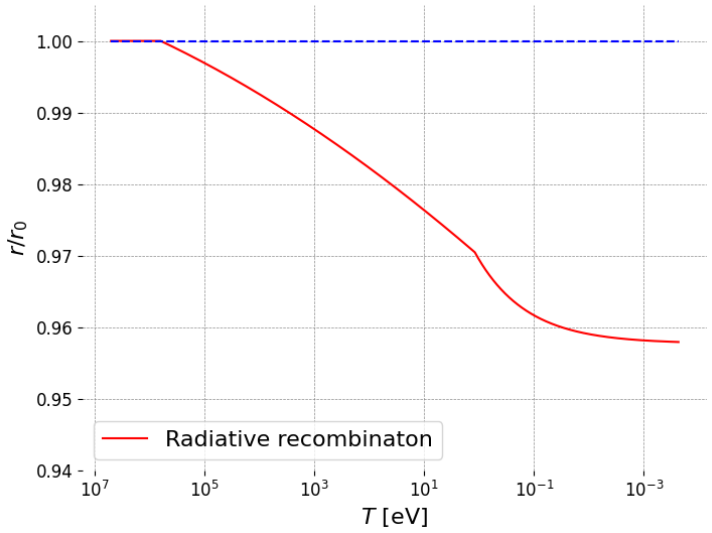


**Figure 2.** Detailed view of the relative density of $y$-charged particles as a function of photon temperature for Kramers recombination. Approximately 4% of the particles transition into a bound state by the present time, providing a more transparent representation of Kramers recombination behavior that is less visible in Figure 1.

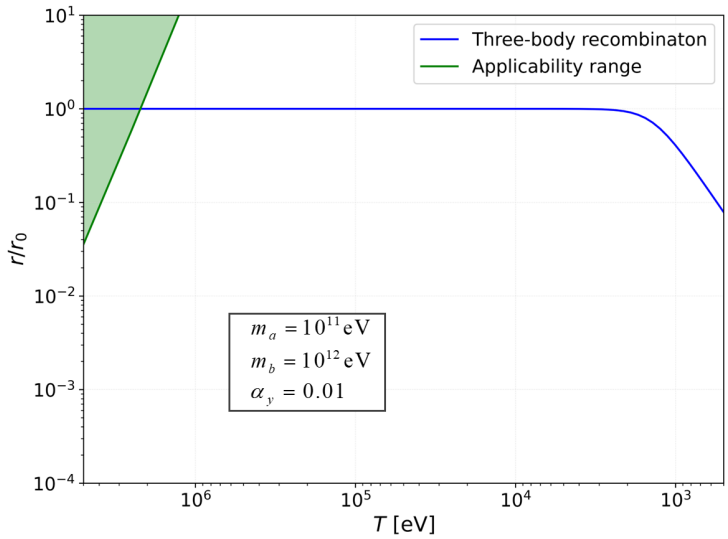


**Figure 3.** Dependence of the relative density of $y$-charged particles on the temperature of photons. The shaded area above the green line represents the region where the three-body recombination formula (11) is valid. As shown, for the current model parameters (Table 1), the density of particles lies below this applicability threshold (13), indicating that the three-body recombination formula is not suitable under these conditions.

### *3.2. Region of Applicability*

The parameters considered in our model do not meet the conditions required for the applicability of the three-body recombination formula. However, adjustments to the self-interacting DM parameters, such as particle masses and interaction constant, could potentially satisfy these conditions. Here, we analyze the parameter space of our model. Specifically, we examine the effects of varying the mass of particle $a$ ($m_a$) and the interaction constant ($\alpha_y$) while keeping the mass of particle $b$ ($m_b$) fixed at 10 times the mass of particle $a$ (i.e., $m_b = 10m_a$).

For different sets of parameters, we calculated the relative density of unbound DM particles using the three-body recombination formula (11), and compare it with constraints on its applicability. The intersection of these functions then indicates the fraction of particles that transitioned to a bound state before the formula's applicability ($r_{3\text{body}}(T_*) = r_{\text{lim}}(T_*) = r_{\text{rec}}$, where $T_*$ denotes the temperature at which the equality of the rates holds, and $r_{\text{lim}}$ is the limiting recombination rate attainable at the last moment of the model's applicability). The resulting relative densities were mapped to the corresponding parameter values to visualize the impact of varying model parameters $m_a$ and $\alpha_y$ on the recombination process.

The results are illustrated in Figure 4 which demonstrates that significant recombination occurs for large interaction constant ($\alpha_y > 1$) and particle masses. To visualize the recombination process under conditions (13) where the three-body recombination formula (11) is valid, Figure 5 is depicted. Figure 5 shows that, while some particles transition to bound states, other particles remain ionized. Such a two-component dark plasma model may potentially explain the positron anomaly.

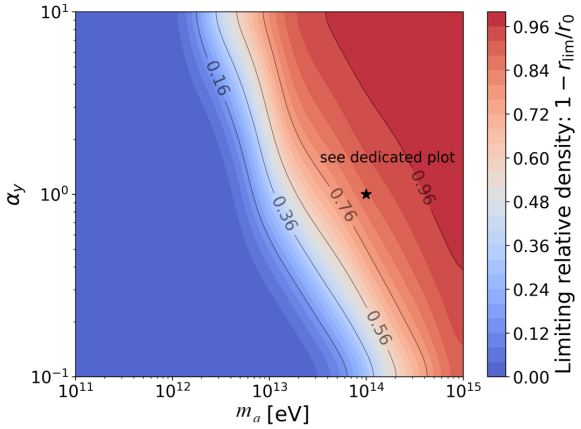


**Figure 4.** Distribution of the limiting relative densities of recombined $y$-particles as a function of the particle mass $m_a$ and the interaction constant $\alpha_y$. The mass of particle $b$ ('dark proton') is fixed at 10 times the mass of particle $a$ ($m_b = 10m_a$). Each value represents the order of magnitude of the relative density of particles that recombined while the three-body recombination formula (11) was applicable. The relative density for the marked parameter set (solid star) is given in Figure 5.

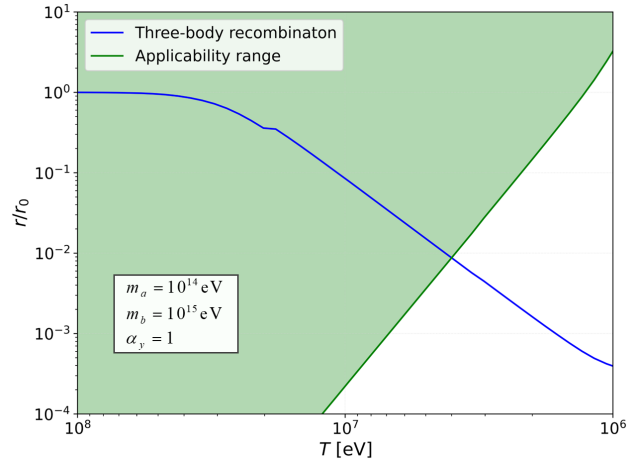


**Figure 5.** Dependence of the relative density of $y$-charged particles on the temperature of photons with a restriction on the applicability (13) of the formula (11). With the parameters used as indicated, less than 1% of the particles remain ionized by the time the three-body recombination formula becomes inapplicable.

### 3.3. Constraints on Model Parameters from Observations

To constrain the parameters of our model, we used the data obtained from experimental observations [38]. Observational constraints on the self-interaction cross-section ($\sigma$) are typically expressed in terms of the ratio $\sigma/m$, where $m$ is the mass of the DM particles. The key approaches used to derive these constraints are as follows:

- Dwarf Galaxies. Dwarf spheroidal galaxies (dSph) represent exceptionally sutable test cases for SIDM models since their dynamics and structure are almost entirely determined by DM, with minimal influence from baryons. In SIDM models, the formation of cores is connected with the redistribution of momentum in the central regions, which smooths out the density profile. Density profiles are reconstructed using stellar velocity dispersion data, which reveal how stars move in the gravitational potential of the galaxy, thereby providing an indirect probe of the underlying DM distribution. Matching observed density profiles to SIDM predictions constrains $\sigma/m$ to the range $0.1\,\mathrm{cm}^2/\mathrm{g} < \sigma/m < 1\,\mathrm{cm}^2/\mathrm{g}$. If $\sigma/m$ is exceptionally large, the core becomes excessively large, inconsistent with observations. Conversely, if $\sigma/m$ is considerably small, the density profile remains cusped, which also contradicts the data [7,39].
- Observations of cluster collisions (for example, the Bullet Cluster). During cluster collisions, gas and stars behave differently: hot gas is slowed by pressure, while stars and DM pass through largely unaffected. The DM distribution is reconstructed using gravitational lensing, which reflects the mass distribution in the cluster. If DM self-interactions are excepionally strong, the DM distribution would show observable discrepancies. Observations of the Bullet Cluster indicate that any offsets between DM and stellar distributions are minimal, constraining $\sigma/m \lesssim 0.1\,\mathrm{cm}^2/\mathrm{g}$ to maintain consistency with the data [40,41].
- Weak Gravitational Lensing. Weak gravitational lensing provides a method for constraining the properties of dark matter, including its self-interactions, by studying the distortion of light from background galaxies as it passes through the gravitational potential of foreground structures. SIDM models predict that self-interactions lead to more spherical halos compared to the triaxial shapes expected in CDM models. This effect becomes observable in the alignment and ellipticity of lensing signals, particularly in massive structures like galaxy clusters. Using precise measurements of weak lensing, recent studies have placed upper limits on $\sigma/m$ by comparing the observed ellipticity distribution of dark matter halos with simulations. For example, constraints derived in Ref. [42] limit $\sigma/m$ to values less than $0.1\,\mathrm{cm}^2/\mathrm{g}$ for galaxy clusters.

The constraints discussed above are typically expressed as limits on the parameter $\sigma/m$, assuming a fixed cross-section independent of velocity. However, in our model, the interaction cross-section is described by the Rutherford formula and explicitly depends on the relative velocity $v$:

$$\sigma(v) = \frac{4\pi e_y^4}{m^2 v^4} = \frac{4\pi(\hbar c)^2 \alpha_y^2}{(mc^2)^2 (v/c)^4} = \frac{4\pi(200\ \mathrm{GeV\ fm})^2 \alpha_y^2}{(mc^2)^2 (v/c)^4}, \tag{14}$$

where $\alpha_y$ is the effective dark Coulomb charge.

To perform a straightforward estimation of the model parameters, we assume that the relative velocity $\bar{v} \approx 200\,\mathrm{km/s}$. Then, the corresponding ratio reads

$$\frac{\sigma(\alpha_y, m)}{m_a} = \frac{\alpha_y^2}{m_a^3 \bar{v}^4} = 1.43 \times\ \mathrm{cm}^2/\mathrm{g} \left(\frac{100\,\mathrm{GeV}}{m_a}\right)^3 \left(\frac{\alpha_y}{0.01}\right)^2 \left(\frac{200\,\mathrm{km/s}}{\bar{v}}\right)^4, \tag{15}$$

Using the velocity-dependent formula (15), we calculated the cross-section for various values of $m$ (in units of GeV) and $\alpha_y$ for a fixed velocity $v = 200\,\mathrm{km/s}$. By normalizing the result to the ratio $\sigma/m$, we then compare the obtained values with the observational constraints discussed just above.

Using the simplified estimation (15) of the cross-section, we overlay the results on the parameter space as shown in Figure 6. Our approach gives a first constraint on the model parameters, but the method has distinct limitations. The assumption of a constant relative velocity $v = 200\,\mathrm{km/s}$ simplifies the problem but neglects variations in velocity distributions across different astrophysical environments. Additionally, the observational constraints we use are averaged over large scale structure and may not capture the complexities of small-range structures.

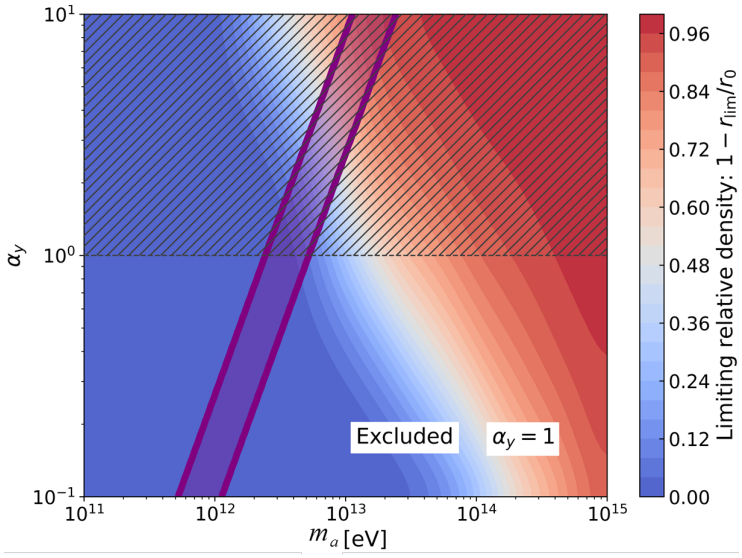


**Figure 6.** Dependence of the relative density of recombined particles on model parameters, where experimental constraints (purple strip) indicate the allowed parameter space. The regions outside the purple strip are disfavored. The hatched region above the dashed horisontal line ($\alpha_y = 1$) corresponds to a strong coupling ($\alpha_y > 1$) regime and should be considered approximate (see text).

The constraints considered in the strong coupling regime [43] ( $\alpha_y > 1$, indicated by the hatched area in Figure 6) should be considered approximate. The Rutherford formula (14) becomes suppressed by inelastic radiation processes, and the Born approximation becomes invalid (while the classical formula remains valid). It is also worthy to emphasize that the constraints derived here assume that all DM is self-interacting. In our model, however, only a fraction of DM remains charged after three-body recombination, while the majority of DM particles recombine into a neutral state and become effectively collisionless. Elastic collisions among these neutral particles are expected to have a considerably large mean free path, further reducing their impact on structure formation. As a result, the derived constraints may overestimate the actual impact of self-interactions in the scenario we comsider.

Nevertheless, this estimation serves as a valuable starting point for identifying regions of parameter space where the three-body recombination process could significantly contribute to DM dynamics. Further refinements to the model and observational data are necessary to improve the accuracy of these constraints.

## 4. Conclusions

We developed a cosmological framework for three-body recombination in a dark-sector U(1) model with a ‘dark electron’ and a ‘dark proton’. On this basis, we de-

rived analytic solutions for the charged fraction across radiation- and matter-dominated epochs—Equations (11) and (12) — which can be confronted with numerical results.

A search for optimal model parameters in $(m_a, \alpha_y)$ plane (Figure 4) illustrates how increasing the interaction constant and the 'dark electron' mass enhances the recombined fraction. Our analysis also reveals that, within a short temperature interval, $T \simeq 10^8$–$10^6$ eV, less than 1% of particles may remain ionized (Figure 5). However, worthy to note that these conditions require unrealistically high values for the interaction constant $\alpha_y$, which may not be characteristic of SIDM. Consequently, while the three-body recombination process demonstrates the potential for nearly complete recombination under these specific conditions, such extreme parameter values might not be physically realistic.

Overall, these results show that three-body recombination can, under appropriate conditions, convert a substantial portion of the interacting dark sector into neutral states. This naturally points to a two-component dark-matter scenario in which a mostly neutral, collisionless component coexists with an interacting fraction. Such a configuration can serve as a foundation for dark matter explanation of the positron anomaly [19,21].

## 5. Discussion

While most cosmological studies rely on the Kramers recombination mechanism to describe recombination processes, alternative mechanisms from plasma physics may also be relevant under certain conditions. Exploring these alternative mechanisms, such as the three-body recombination process discussed in this study, might provide interesting results. New mechanisms could provide new insights and potentially resolve existing discrepancies in our current models of dark matter.

The three-body recombination process demonstrates a significantly faster transition of particles into bound states compared to the Kramers recombination. This enhanced efficiency depends on certain conditions, such as high particle density. This finding highlights the need for sufficiently large particle densities (such as in clusters) or alternative parameter choices to realize the potential advantages of three-body recombination.

While the three-body recombination process holds promise, its applicability is limited by stringent conditions. Specifically, the particle density must be sufficiently high for the process to occur. In our model, the required densities or parameter values might not be physically realistic for SIDM. Nonetheless, the results suggest that under appropriate conditions, three-body recombination may significantly contribute to the number of bound states, potentially outperforming other mechanisms.

Future study should expand the interaction models beyond the dark Coulomb case (for example, Yukawa-mediated or other potentials). On the computational side, the present treatment solves a single differential equation for the $y$-charged particles, but a more accurate approach would solve a coupled system for $n_a$ and $n_b$ that also includes reverse ionization. Astrophysically, three-body recombination may become efficient in regions with higher DM density, so applying the same three-body framework to such environments is a natural next step. Finally, constraints on SIDM should be reformulated for a two-component dark sector, with limits given in terms of the transport cross-section per unit mass and the remaining charged fraction, so that observational bounds can be mapped consistently onto models with a comparably large neutral component.

**Author Contributions:** Conceptualization, K.B. and D.K.; writing—original draft, D.K.; writing—revew and editing, K.B. and D.K.; software, D.K.; validation, D.K. and K.B.; visualization, D.K.; supervision, K.B.; project administration, K.B.; funding acquisition, K.B. and D.K. All authors have read and agreed to the published version of the manuscript.

**Funding:** This research was funded by Russian Science Foundation grant no. 24-22-00325 *Search for an explanation of the positron anomaly in cosmic rays by means of dark matter*.

**Data Availability Statement:** The data presented in this study are available on reasonable request from the corresponding author.

**Acknowledgments:** We thank Katerina Esipova for valuable discussions and for help in shaping the logic of the calculations.

**Conflicts of Interest:** The authors declare no conflict of interest.

## References

1. Ghigna, S.; Moore, B.; Governato, F.; Lake, G.; Quinn, T.; Stadel, J. Density profiles and substructure of dark matter halos: Converging results at ultra-high numerical resolution. *Astrophys. J.* **2000**, *544*, 616–628. [CrossRef]
2. Klypin, A.; Kravtsov, A.V.; Valenzuela, O.; Prada, F. Where are the missing galactic satellites? *Astrophys. J.* **1999**, *522*, 82–92. [CrossRef]
3. Spergel, D.N.; Steinhardt, P.J. Observational evidence for self-interacting cold dark matter. *Phys. Rev. Lett.* **2000**, *84*, 3760–3763. [CrossRef]
4. Wandelt, B.D.; Davé, R.; Farrar, G.R.; McGuire, P.C.; Spergel, D.N.; Steinhardt, P.J. Self-interacting dark matter. In *Sources and Detection of Dark Matter and Dark Energy in the Universe: Fourth International Symposium Held at Marina del Rey, CA, USA, February 23-25, 2000*; Cline, D.B., Ed.; Springer: Berlin/Heidelberg, Germany, 2001; pp. 263–274. [CrossRef]
5. Rubakov, V.A. Cosmology and dark matter. Lectures at European School on High Energy Physics *ESHEP2019*, Saint-Petersburg, Russia, 4–17 September 2019. *arXiv* **2019**, arXiv:1912.04727. [CrossRef]
6. Randall, L.; Scholtz, J. Dissipative dark matter and the Andromeda plane of satellites. *J. Cosmol. Astropart. Phys.* **2015**, *2015*, 057. [CrossRef]
7. Tulin, S.; Yu, H.B. Dark matter self-interactions and small scale structure. *Phys. Rep.* **2018**, *730*, 1–57. [CrossRef]
8. Shen, X.; Hopkins, P.F.; Necib, L.; Jiang, F.; Boylan-Kolchin, M.; Wetzel, A. Dissipative dark matter on FIRE— I. Structural and kinematic properties of dwarf galaxies. *Mon. Not. R. Astron. Soc.* **2021**, *506*, 4421–4445. [CrossRef]
9. Alonso-Álvarez, G.; Cline, J.M.; Dewar, C. Self-interacting dark matter solves the final parsec problem of supermassive black hole mergers. *Phys. Rev. Lett.* **2024**, *133*, 021401. [CrossRef]
10. Adriani, O.; Barbarino, G.C.; Bazilevskaya, G.A.; Bellotti, R.; Boezio, M.; Bogomolov, E.A.; Bonechi, L.; Bongi, M.; Bonvicini, V.; Bottai, S.; et al. An anomalous positron abundance in cosmic rays with energies 1.5–100 GeV. *Nature* **2009**, *458*, 607–609. [CrossRef]
11. Aguilar, M.; et al. [AMS Collaboration] First result from the Alpha Magnetic Spectrometer on the International Space Station: Precision measurement of the positron fraction in primary cosmic rays of 0.5–350 GeV. *Phys. Rev. Lett.* **2013**, *110*, 141102. [CrossRef]
12. Linden, T.; Profumo, S. Probing the pulsar origin of the Anomalous Positron Fraction with AMS-02 and atmospheric Cherenkov telescopes. *Astrophys. J.* **2013**, *772*, 18. [CrossRef]
13. Hooper, D.; Cholis, I.; Linden, T.; Fang, K. HAWC observations strongly favor pulsar interpretations of the cosmic-ray positron excess. *Phys. Rev. D* **2017**, *96*, 103013. [CrossRef]
14. Alekseev, V.V.; Belotsky, K.M.; Bogomolov, Y.V.; Budaev, R.I.; Dunaeva, O.A.; Kirillov, A.A.; Kuznetsov, A.V.; Laletin, M.N.; Lukyanov, A.D.; Malakhov, V.V.; et al. High-energy cosmic antiparticle excess vs. isotropic gamma-ray background problem in decaying dark matter Universe. *J. Phys. Conf. Ser.* **2016**, *675*, 012023. [CrossRef]
15. Liu, W.; Bi, X.-J.; Lin, S.-J.; Yin, P.-F. Constraints on dark matter annihilation and decay from the isotropic gamma-ray background. *Chin. Phys. C* **2017**, *41*, 045104. [CrossRef]
16. Belotsky, K.; Budaev, R.; Kirillov, A.; Laletin, M. Fermi-LAT kills dark matter interpretations of AMS-02 data. Or not? *J. Cosmol. Astropart. Phys.* **2017**, *2017*, 021. [CrossRef]
17. Belotsky, K.M.; Budaev, R.I.; Kirillov, A.A.; Solovyov, M.L. Gamma-rays from possible disk component of dark matter. *J. Phys. Conf. Ser.* **2017**, *798*, 012084. [CrossRef]
18. Belotsky, K.M.; Kirillov, A.A.; Solovyov, M.L. Development of dark disk model of positron anomaly origin. *Int. J. Mod. Phys. D* **2018**, *27*, 1841010. [CrossRef]
19. Belotsky, K.M.; Solovev, M.L. Dark matter with special spatial distribution as possible explanation of positron excess in cosmic rays. *Phys. Part. Nucl.* **2025**, *56*, 599–603. [CrossRef]
20. Belotsky, K.M.; Esipova, E.A.; Kamaletdinov, A.K.; Shlepkina, E.S.; Solovyov, M.L. Indirect effects of dark matter. *Int. J. Mod. Phys. D* **2019**, *28*, 1941011. [CrossRef]

21. Belotsky, K.M.; Solovyov, M.L.; Rakhimova, M.A. Mechanisms of cosmic ray generation. *Phys. At. Nucl.* **2022**, *85*, 92–96. [CrossRef]
22. Zhang, L.; Chen, X.; Lei, Y.-A.; Si, Z.-g. Impacts of dark matter particle annihilation on recombination and the anisotropies of the cosmic microwave background. *Phys. Rev. D* **2006**, *74*, 103519. [CrossRef]
23. Belotsky, K.M.; Esipova, E.A.; Kirillov, A.A. On the classical description of the recombination of dark matter particles with a Coulomb-like interaction. *Phys. Lett. B* **2016**, *761*, 81–86. [CrossRef]
24. Belotsky, K.M.; Esipova, E.A.; Kirillov, A.A. On the temperature evolution of multicomponent dark matter with Coulomb-like interaction. *J. Phys. Conf. Ser.* **2016**, *675*, 012017. [CrossRef]
25. von Harling, B.; Petraki, K. Bound-state formation for thermal relic dark matter and unitarity. *J. Cosmol. Astropart. Phys.* **2014**, *12*, 033. [CrossRef]
26. Petraki, K.; Pearce, L.; Kusenko, A. Self-interacting asymmetric dark matter coupled to a light massive dark photon. *J. Cosmol. Astropart. Phys.* **2014**, *07*, 039. [CrossRef]
27. Chu, X.; Hambye, T.; Tytgat, M.H.G. The four basic ways of creating dark matter through a portal. *J. Cosmol. Astropart. Phys.* **2012**, *05*, 034. [CrossRef]
28. Alexander, J.; Battaglieri, M.; Echenard, B.; Essig, R.; Graham, M.; Izaguirre, E.; Jaros, J.; Krnjaic, G.; Mardon, J.; Morrissey, D.; et al. Dark Sectors 2016 workshop: Community report. *arXiv* **2016**, arXiv:1608.08632. [CrossRef]
29. Belotsky, K.; Khlopov, M.; Kouvaris, C.; Laletin, M. High-energy positrons and gamma radiation from decaying constituents of a two-component dark atom model. *Int. J. Mod. Phys. D* **2015**, *24*, 1545004. [CrossRef]
30. Belotsky, K.; Khlopov, M.; Kouvaris, C.; Laletin, M. Decaying dark atom constituents and cosmic positron excess. *Adv. High Energy Phys.* **2014**, *2014*, 214258. [CrossRef]
31. Belotsky, K.M.; Khlopov, M.Y.; Legonkov, S.V.; Shibaev, K.I. Effects of new long-range interaction: Recombination of relic Heavy neutrinos and antineutrinos. *Grav. Cosmol.* **2005**, *11*, 27–33. [CrossRef]
32. Belotsky, K.; Esipova, E.; Kalashnikov, D.; Letunov, A. Problems of the correspondence principle for the recombination cross section in dark plasma. In *Proceedings of the 23rd Workshop "What Comes Beyond the Standard Models", Bled, July 4–12. 2020 [Virtual Workshop. July 6.-10.2020]. Volume 2: Further Talks and Scientific Debuts*; Mankoč Borštnik, N.S., Nielsen, H.B., Lukman, D., Eds.; DMFA—Založištvo: Ljubljana, Slovenia, 2020; pp. 77–83. Available online: http://bsm.fmf.uni-lj.si/bled2020bsm/talks/BledVol21No2Proceedings-proc20Vol2.pdf (accessed on 23 November 2025).
33. Barabanov, A.L.; Belotsky, K.M.; Esipova, E.A.; Kalashnikov, D.S.; Letunov, A.Y. On quantum and classical treatments of radiative recombination. *Phys. Lett. B* **2022**, *834*, 137459. [CrossRef]
34. Pitaevskiĭ, L.P. Electron recombination in a monoatomic gas. *Zh. Eksp. Teor. Fiz. (ZhETF)* **1962**, *42*, 1326–1329; English translation: *Sov. Phys. JETP* **1962**, *15*, 919–921. Available online: http://jetp.ras.ru/cgi-bin/e/index/e/15/5/p919?a=list (accessed on 23 November 2025).
35. Knyazev, B.A. *Low-Temperature Plasma and Gas Discharge*; Novosibirsk State University: Novosibirsk, Russia, 2003. (In Russian)
36. Belotsky, K.M.; Esipova, E.A.; Khlopov, M.Y.; Laletin, M.N. Dark Coulomb binding of heavy neutrinos of fourth family. *Int. J. Mod. Phys. D* **2015**, *24*, 1545008. [CrossRef]
37. Bansal, S.; Barron, J.; Curtin, D.; Tsai, Y. Precision cosmological constraints on atomic dark matter. *J. High Energy Phys.* **2023**, *2023*, 95. [CrossRef]
38. Cirelli, M.; Strumia, A.; Zupan, J. Dark matter. *SciPost Phys. Rev.* **2026**, *1*, 1-689. [CrossRef]
39. Bullock, J.S.; Boylan-Kolchin, M. Small-scale challenges to the ΛCDM paradigm. *Annu. Rev. Astron. Astrophys.* **2017**, *55*, 343–387. [CrossRef]
40. Markevitch, M.; Gonzalez, A.H.; Clowe, D.; Vikhlinin, A.; Forman, W.; Jones, C.; Murray, S.; Tucker, W. Direct constraints on the dark matter self-interaction cross section from the merging galaxy cluster 1E 0657-56. *Astrophys. J.* **2004**, *606*, 819–824. [CrossRef]
41. Robertson, A.; Massey, R.; Eke, V. What does the Bullet Cluster tell us about self-interacting dark matter? *Mon. Not. R. Astron. Soc.* **2016**, *465*, 569–587. [CrossRef]
42. Adhikari, S.; Banerjee, A.; Jain, B.; Shin, T.-h.; Zhong, Y.-M. Constraints on dark matter self-interactions from weak lensing of galaxies from the Dark Energy Survey around clusters from the Atacama Cosmology Telescope Survey. *Astrophys. J.* **2015**, *983*, 50. [CrossRef]
43. Müller, B.; Peitz, H.; Rafelski, J.; Greiner, W. Solution of the Dirac equation for strong external fields. *Phys. Rev. Lett.* **1972**, *28*, 1235–1238. [CrossRef]